Measuring heat capacity of activated carbons for CO_2 capture

N. Querejeta[1,2], S. García[2], N. Álvarez-Gutiérrez[1], F. Rubiera[1], C. Pevida[1]*

[1] Instituto Nacional del Carbón, INCAR-CSIC, c/ Francisco Pintado Fe 26, 33011 Oviedo, Spain

[2] Research Centre for Carbon Solutions (RCCS), School of Engineering & Physical Sciences, Heriot-Watt University, Edinburgh EH14 4AS, UK

Abstract

Capturing CO_2 with solid adsorbents can be often limited by heat transfer during the regeneration process rather than mass transfer during the adsorption process. The use of a low-heat capacity adsorbent would result in a lower energy penalty for the regeneration step. Specific heat capacity (*Cp*) data knowledge of solid adsorbents is still scarce in the literature. To gather information in this regard, activated carbons (ACs) prepared from different precursor materials, synthesis conditions, activating agents and surface modifications have been experimentally tested. The specific heat capacity has been evaluated at temperatures ranging from 50 to 190 °C, relevant for temperature swing adsorption (TSA) based CO_2 capture processes. A thermogravimetric analyser/differential scanning calorimeter (TGA/DSC) has been used for the experimental testing. *Cp* values of the evaluated adsorbents evidenced significant dependency on temperature: adsorbents either showed a linear upward trend with temperature –phenolic resin-derived ACs- or they peaked at a determined temperature range –biomass based ACs-. This peak has been ascribed to oxidation reactions of biomass based carbons during the experiment. It is noteworthy that adsorbent surface modification plays a key role in the specific heat capacity of the resultant carbon. Likewise, the acid and basic character of the carbon surface has been identified as key parameter for effective regeneration in TSA processes. AC adsorbents with an acidic character are undesirable owing to their higher specific heat capacities.

Keywords: heat capacity; activated carbon; temperature swing adsorption; CO_2 capture.

1 Introduction

Sorption-based processes offer some advantages over conventional amine scrubbing for CO_2 capture including lower energy requirements in regeneration, no liquid waste production and a much wider range of operating temperatures (typically ranging from ambient to 700 °C). Low-temperature (≤ 200 °C) solid sorbents currently considered for CO_2 capture include activated carbons, ion-exchange resins, silica gel, activated alumina, and surface-functionalized nanoporous materials based on silica and carbon [1]. Amongst those, carbon-based adsorbents are considered highly promising due to attributes such as low cost, high surface area, high amenability to pore structure modification and surface functionalisation, and relative ease of regeneration [2–7].

*Corresponding author. Tel.: +34 985 11 89 87
E-mail address: cpevida@incar.csic.es (C. Pevida)

Although adsorption technology is not fully deployed at commercial scale for CO_2 capture as yet, the intensive research and development activity along with the sharp increase in the number of patents filled in recent years point that this technology is emerging [8,9,18–20,10–17]. Solid adsorbents are usually packed as fixed beds and employed in unsteady cyclic processes composed of adsorption and regeneration steps. The regeneration or desorption step is often the cost-determining factor of the separation process. The mechanism of CO_2 adsorption on carbon-based adsorbents is mainly attributable to weak physical forces, which makes regeneration of spent adsorbents at a relatively low temperature (≤ 200 ˚C) feasible. The application of activated carbons to CO_2 capture has been extensively studied. Activated carbons benefit from industrial maturity, are generally cheap and can be manufactured at large scale. Owing to their hydrophobic nature, activated carbons are not strongly affected by moisture, though a decrease in capacity is often observed compared to the performance under dry conditions [21]. A major challenge for the deployment of CO_2 capture by means of adsorption on activated carbons at large scale includes the lower selectivity towards CO_2, compared to other adsorbents such as zeolites or MOFs, that increases the carbon footprint.

When evaluating and comparing adsorbents for use in commercial-scale CO_2 capture systems, it is important to determine those parameters that are expected to have considerable impact on the process efficiency. Suitable adsorbent selection criteria must consider all the relevant sorption properties. However, specific targets for CO_2 capture materials, for instance, working capacity, selectivity, sorption rates, enthalpies of sorption [22], heat capacity, attrition resistance or stability to acid gases have not been clearly stablished. One of the most important evaluation criteria to select a suitable adsorbent is the energy required for regeneration. However, heat capacity is a property scarcely reported for solid adsorbents despite it being essential to estimate energy requirements for regeneration in thermal swing operation [11].

In cyclic temperature swing adsorption (TSA) operation where adsorbent regeneration is conducted by a thermal swing, the adsorbent is heated up to the desired desorption temperature. Then the thermal energy required is the sum of the sensible heat needed to heat the bed to the desorption temperature, i.e., sensible heat (Q_{sen}), and the energy needed to overcome the heat of desorption (Q_{des}) [23]. The sensible heat is calculated as: $Q_{sen} = m \cdot Cp \cdot \Delta T$, where m is the mass of adsorbent (in kg), Cp the specific heat of adsorbent (in kJ/(kg ˚C)), and ΔT the temperature difference (in degrees Celsius) between the regeneration and adsorption steps. If an isobaric process with direct-steam stripping is considered, the energy requirements to heat the adsorbent can account for up to 90% of the steam energy demand [7]. Hence, the heat capacity of the adsorbent will impact the energy penalty of the heating process which, in turn, would either increase or decrease the total energy requirements of the CO_2 separation. A low-heat capacity adsorbent will then help to reduce the total cost of CO_2 capture [13,24,25].

Heat capacity data of solid adsorbents not only thermodynamically characterise the material, they should also be taken into account when optimising the CO_2 separation process. Furthermore, gathering of data such as heat of desorption, specific heat, mass-transfer and diffusional effects is also

essential for candidate adsorbents being developed and for the design of CO_2 removal systems. However, at the current state of development, most of these characteristics are not openly accessible [2].

We report a detailed study on heat capacity (*Cp*) measurements of a large array of activated carbons previously synthesised for CO_2 capture under different operating conditions. To the best of the authors' knowledge, an experimental study like the one herein has not been reported in literature.

2 Materials and methods

2.1 Materials

Ten adsorbents, mainly microporous activated carbons (ACs), have been selected to conduct the experimental study. Materials include ACs from different carbon precursors, synthesis conditions, activating agents and adsorbent surface modifications, spanning a wide range of properties to account for their influence on heat capacity measurements.

Table 1. Preparation conditions for the selected ACs.

Adsorbent	Precursor	Type	Treatment	Agent	T (°C)	Ref.
CLA	PF[1]	Novolac	PA[4]	CO_2	900	[26]
CLOS	PF+Biomass	Novolac+ OS[2]	PA	CO_2	940	[27]
E1	PF	Novolac	PA	CO_2	800	[26]
GPF	PF	Resol	PA	CO_2	900	[26]
GKAS	Biomass	AS[3]	Carbonization	N_2	600	[28]
GKASA	GKAS	--	PA	CO_2	700	[29]
GKASN	GKAS	--	Amination	NH_3	800	[29]
Norit C	Biomass	Wood	CA[5]	H_3PO_4	550	[30]
CN	Norit C	--	Amination	NH_3	800	[31]
CNO	Norit C	--	Ammoxidation	NH_3 +Air	300	[32]

1. Phenol-formaldehyde resin; 2. Olive stones; 3. Almond shells; 4. Physical activation; 5. Chemical activation

A commercial granular activated carbon, Norit C, was included in the array of samples to be tested as reference material for benchmarking purposes. A summary of the preparation conditions for each adsorbent is presented in Table 1. The adsorbents were produced/purchased in granular form but were ground manually (mortar and pestle) to produce a fine powder (~ 212 μm) that could be uniformly compacted in the pan for the Cp measurements. Therefore, all samples were evaluated in powder form in order to avoid the influence of different particle sizes and morphologies on the measurements [33].

2.2 Heat capacity measurements

Among the several techniques available, differential scanning calorimetry (DSC) is considered a powerful tool to accurately measure the specific heat capacity of samples at milligram level due to its speed and simplicity [33]. DSC tests consist of heating the sample at a controlled rate in a specified environment over the temperature range of interest. The difference in heat flow between the sample and a reference material, owing to energy changes, is continuously monitored and recorded. The DSC signal measurement and the dynamic mode of operation are the two main features of this technique [34].

At constant pressure, the specific heat capacity (*Cp*) is a measure of the amount of energy required to raise the temperature of 1 g (or 1 mol) of a substance by 1 °C. In DSC, the measured heat flow is directly proportional to the *Cp*, which allows its calculation directly from the DSC signal.

In this study, heat capacity measurements were performed in a thermogravimetric analyser/differential scanning calorimeter, TGA/DSC1 STARe System from Mettler Toledo. The thermogravimetric analyser accurately controls the temperature and the heating rate of the sample and the reference material. Experiments were conducted in inert atmosphere by flowing nitrogen at a controlled flow rate of 50 mL min^{-1}. Platinum pans with a volumetric capacity of 70 µL and the corresponding lids were used in the testing.

2.2.1 Sapphire method

The DSC system was calibrated using sapphire as the standard reference material for *Cp* determination. This is a standard procedure described in ASTM E1269 [23].

In this method, the DSC signal of the sample is compared with the DSC signal of the reference sapphire sample of known specific heat capacity. Both curves need to be blank-curve corrected. Thus, the first measurement determines the DSC signal of the empty sample crucible and in the second, either the sapphire or the adsorbent is placed into the crucible and the DSC signal of the whole ensemble is measured. The net DSC signal is then calculated by difference between both measurements.

The mathematical–statistical processing of the experimental DSC data to obtain the specific heat capacities corresponding to the sapphire in the temperature range evaluated, consisted in fitting the set of data to a polynomial function by means of the following equation proposed by Ditmars et al [35]:

$$y = 9e^{-16}x^5 - 4e^{-12}x^4 + 6e^{-9}x^3 - 5e^{-6}x^2 + 0.024x + 0.7121 \quad (1)$$

where *y* stands for the specific heat capacity of the sapphire in J/g °C and *x* stands for the temperature evaluated in °C.

At constant pressure, individual *Cp* values at different temperatures can be determined from the recorded DSC data according to the following equation:

$$Cp(T) = \frac{DSC_{adsorbent} - DSC_{blank}}{DSC_{sapphire} - DSC_{blank}} \cdot Cp_{\,sapphire} \quad (2)$$

in which *Cp(T)* is the specific heat capacity of the evaluated sample at temperature T; *($DSC_{adsorbent}$ - DSC_{blank})* is the net DSC signal of the sample after blank correction; *($DSC_{sapphire}$ -DSC_{blank})* is the net DSC signal of the reference material (sapphire) after blank correction and $Cp_{sapphire}$ is the specific heat capacity of the standard reference material (sapphire) obtained by fitting the experimental data to Equation 1.

2.2.2 Experimental procedure

Series of runs were conducted in the TGA/DSC1 thermogravimetric analyser to evaluate the specific heat capacities of the selected ACs by means of the sapphire method described above. Firstly, blank measurements were carried out using covered, i.e., with lids, empty sample pans; secondly, a standard synthetic sapphire disk (with known specific heat capacity and mass) was used as the reference

material to calibrate the heat flow rate; lastly, sample measurements were performed replacing the reference material with approximately 25 mg of each activated carbon. As the samples were tested in powder form, particular care was taken to ensure good thermal contact. Hence, powdery samples were manually compacted with a DSC tool available for this purpose to ensure that a thin layer without void spaces was filling the bottom of the pan. It is important to note that the pans were not sealed with the lids [34]. The use of a lid gives a constant-emissivity package, independent of the pan content, and meaningful heat capacities are readily obtained [36]. With hermetically sealed pans the DSC signal might not be affected by sublimation and evaporation [37].

All runs followed the same experimental protocol that was adapted from Mu et al. [38]. Before each experiment the adsorbent was dried by heating at 20 °C min^{-1} from ambient temperature up to 105 °C, at atmospheric pressure, and the temperature was held constant at 105°C for 60 min. Drying was conducted in flowing N_2 (50 mL min^{-1}). Samples were then subjected to three consecutive cycles: the first two aim at conditioning the measuring cell and the third cycle is then used for the determination of the heat capacity with better accuracy. DSC and temperature profiles of a representative experiment are shown in Figure 1.

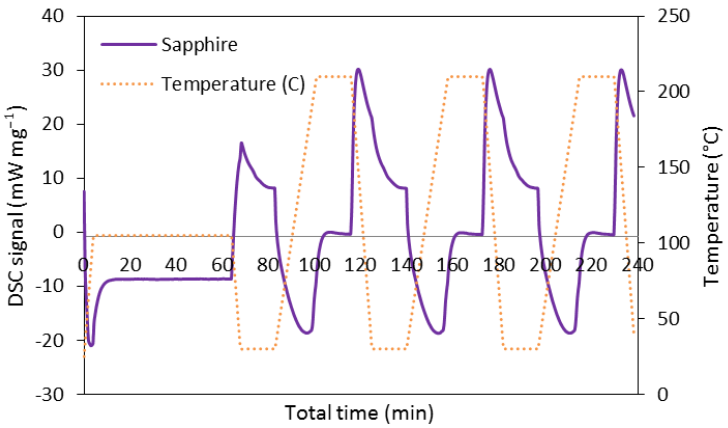

Figure 1. DSC signal and temperature *vs.* time for a representative *Cp* experiment.

Each cycle involved the following segments: The first segment is the cooling of the sample down to 30 °C at a cooling rate of 20 °C min^{-1}. The second segment is a preconditioning step for 15 min at this initial temperature (30 °C). The third segment heats the sample from the initial temperature up to the final temperature (210 °C). A heating rate of 10 ° C min^{-1} is maintained throughout this segment. The final segment is isothermal at this final temperature of 210 °C for 15 min. In order to maintain a dry and inert atmosphere, 50 mL min^{-1} of N_2 were allowed to flow through the system in each cycle. This sweeping gas ensures removal of gases that might be released upon heating the porous samples.

3 Results and discussion

3.1 Heat capacity measurements

As explained in Section 2.2.2, samples were subjected to three consecutive cycles but only the third scan was used in the calculation of *Cp* values for accuracy in the estimation [38].

The DSC technique in which the rate of temperature change is continuously monitored and correlated to the heat flow rate is subject to thermal lag, which is the difference between the temperature of the sensor in the instrument and the mean sample temperature under dynamic (measurement) conditions [39]. In addition, the heating or cooling does not take place instantaneously and every sample needs a certain time to attain the isothermal equilibrium [36].

Thus in order to avoid these, let us call them "edge effects", in the calculated results, specific heat capacity values were only estimated for a temperature range between 50 and 190 ˚C where the thermal equilibrium is guaranteed [33]. This temperature range covers the typical operating temperature window for TSA processes.

The influence of different parameters and ACs preparation conditions on the calculated *Cp* values was evaluated and results are presented in the sections below.

3.1.1 Influence of precursor material and ACs preparation conditions

Activated carbons CLA and GPF were obtained from two different precursor resins, Novolac and Resol, respectively. These resins were prepared by means of two synthesis routes: acid (hydrochloric acid, 37 wt.% HCl solution) catalysis for the former and basic (sodium hydroxide, NaOH) catalysis for the latter. Details on the synthesis of both activated carbons are described in Martin et al. [26].

The specific heat capacities profiles of CLA and GPF are presented in Figure 2. *Cp* values follow a linear trend over the 50 to 190 °C temperature range, as already reported by Kano et al. [40], and Uddin et al. [33], for woodceramics specimens and spherical activated carbon KOH6-PR, respectively. The behaviour of CLA and GPF is independent of the phenolic resin that was used as precursor material to produce the adsorbents and thereby of the basic/acid synthesis route followed.

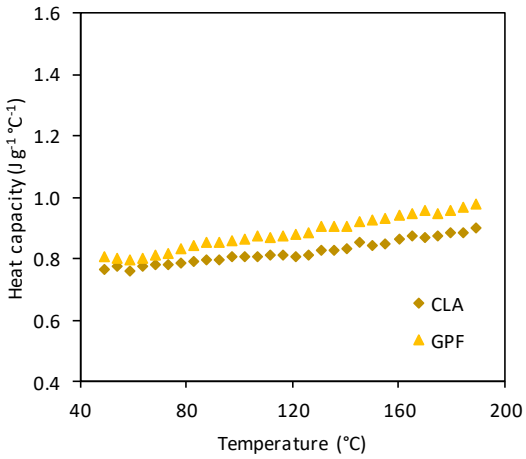

Figure 2. Specific heat capacities of ACs derived from two phenolic resin precursor materials.

Globally, lower *Cp* values are obtained for CLA when compared with GPF over the entire range of studied temperatures, which makes it more suitable for thermal swing adsorption operation.

Two activated carbons produced from the same phenolic resin precursor (Novolac) were also tested in order to assess the influence of the addition of an organic additive, ethylene glycol (1 wt.%), for activated carbon E1, and the mixture with an agricultural by-product, olive stones (80 wt.%), for activated carbon CLOS. The preparation protocols for these two activated carbons are further described elsewhere [26,27].

For comparative purposes, the specific heat capacities of E1 and CLOS are plotted alongside *Cp* values for CLA in Figure 2. The phenolic resin-derived carbon E1 shows the same trend observed above for CLA and GPF (Figure 3a). Thus, the addition of ethylene glycol (1%) prior to the curing step of the Novolac resin does not alter the trend observed in the specific heat capacity of the phenolic carbons with temperature.

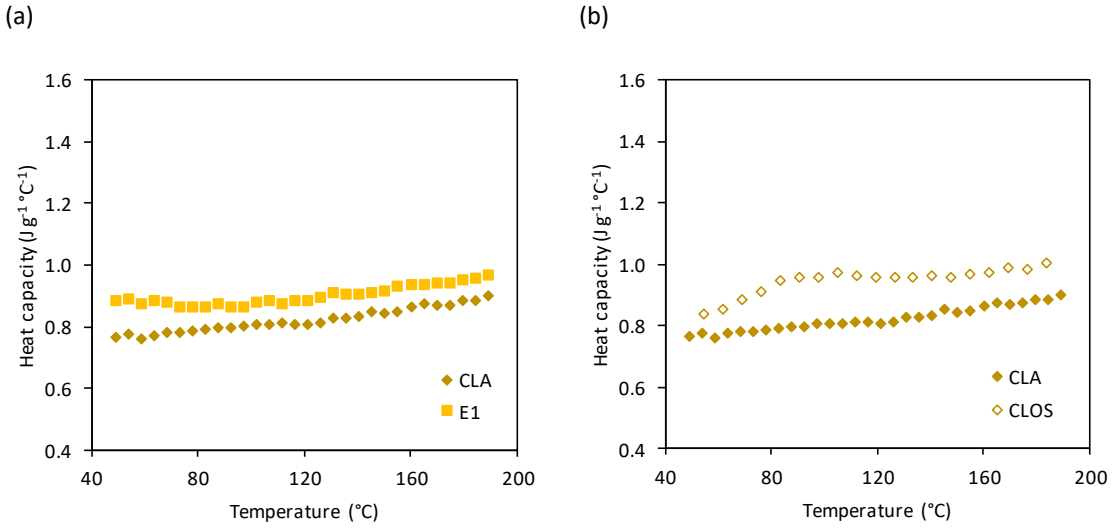

Figure 3. Specific heat capacities of ACs derived from Novolac resin with addition of ethylene glycol (E1) and olive stones (CLOS).

Slightly higher heat capacity values are recorded for E1 compared to CLA.

The trend observed for *Cp* values of activated carbon CLOS shows some changes: a shoulder appears at temperatures between 80 and 120 ˚C. This behaviour could be attributed to the biomass added to the Novolac resin in the formulation of this AC.

To gain more insights into the role of biomass, the specific heat capacity of an activated carbon (GKASA) derived from a different biomass precursor, almond shells [29], was also evaluated in this study.

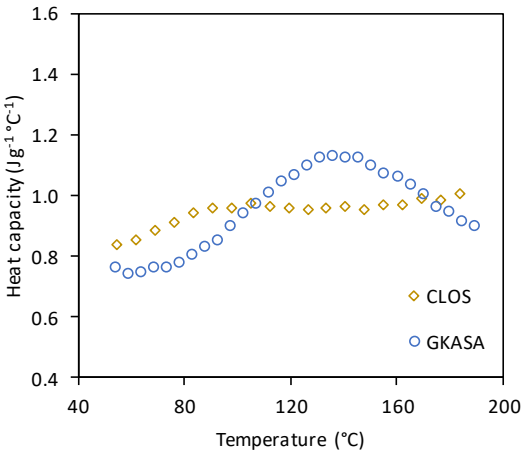

206 **Figure 4.** Specific heat capacities of ACs produced with different biomass precursors.

207 As can be seen in Figure 4, the specific heat capacity of GKASA shows a trend similar to CLOS:
208 there is a peak in the specific heat capacity *versus* temperature curve. However, the peak observed for
209 GKASA is more pronounced and broader, and the maximum is shifted to higher temperature (136 ˚C).
210 In order to understand the aforementioned different trends in *Cp* values, the thermal stability
211 under N_2 atmosphere of the samples was also analysed taking advantage of the thermogravimetric
212 device used in the measurements (TG-DSC). The mass loss profiles (TG and DTG signals) of carbons CLA,
213 CLOS and GKASA during the heat capacity measurement experiments are compared in Figure 5.

(a)

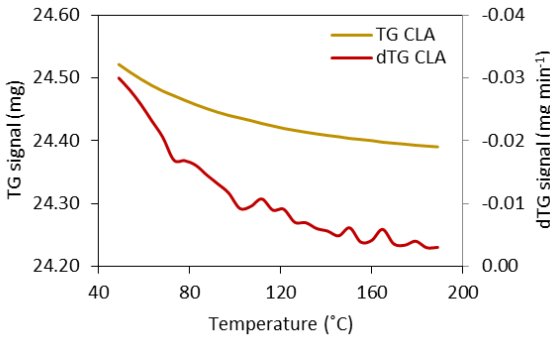

(b)

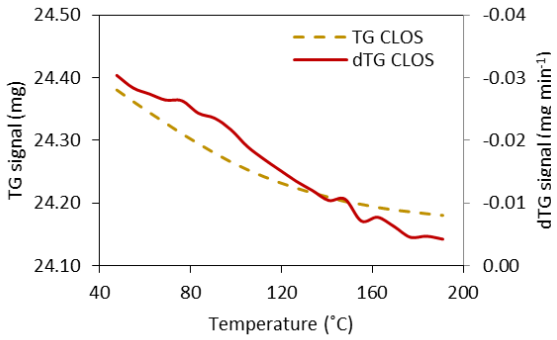

(c)

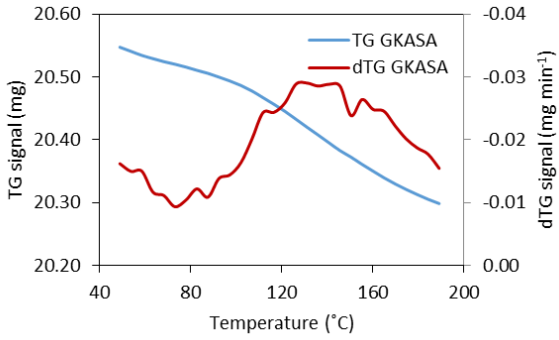

Figure 5. Thermal stability of activated carbons: phenolic resin-derived carbon, CLA (a) and biomass-derived carbons, CLOS (b) and GKASA (c).

Phenol-formaldehyde resin-derived carbon, CLA, shows a weight loss of 0.54% over the whole temperature range evaluated (Figure 5a). This is the expected performance taking into account that the experimental procedure followed in the experimental evaluation of *Cp* includes a preliminary drying step at 105 ˚C, as explained in Section 2.2.2.

The addition of biomass (20 wt.%) to the activated carbon CLOS leads to a slight increase in mass loss and to a change in the shape of the DTG profile, particularly within the 80-120 °C temperature range where specific heat capacity shows a shoulder (Figure 5b).

Activated carbon produced solely from biomass, GKASA, also experiences a reduction in mass upon heating during the experiment; it can be observed that the shape of the TG and DTG profiles have changed and two regions with differentiated slopes can be identified in Figure 5c. It is important to note that even though utmost care was taken to ensure uniform distribution of the powder samples and a closed environment in the pans (lids were used), trace amounts of gases (i.e., air) could remain trapped in between the solid particles and cause oxidation reactions. Products from those reactions could decompose with further rise in temperature, which might result in a variable heat flow and eventually larger uncertainties in *Cp* measurements [33,34], [41,42].

Furthermore, inherent water plays an important role in the oxidation process. A minimum amount of water (about 1 wt.%) is necessary for the interaction between activated carbon and O_2. Biomass-derived carbons are less stable in the presence of moisture and thus possess higher humidity content with regard to that of phenolic resin carbons. Despite the hydrophobic character of activated carbons, the number of hydrophilic groups capable of forming hydrogen bonds with water still remain high in the biomass based carbons [43]. Likewise, some water can be produced as a result of the thermal decomposition occurring in the activated carbons upon heating from 30 ˚C to 210 ˚C. Thus, these oxidation reactions can be considered a side effect due to insufficient drying of the biomass based carbons. Other authors have reported a more intensive drying protocol [33]. In addition, the use of a lid covering the crucible could prevent the evaporation of moisture and difficult the complete removal of inherent water in the samples [37].

Temperature also has a significant effect on the oxidation process: higher temperatures enhance the rate of activated carbon oxidation and result in a higher level of emission of oxygenated compounds [44]. Studies normally consider a temperature range between ambient and 100 ˚C for the oxidation of carbon materials to take place. Sometimes, this range is extended to 150 ˚C [41], which corresponds to the behaviour observed in the studied samples. In addition, it has been reported that the rate of oxygen consumption almost doubles with a rise in temperature of only 10 ˚C [41].

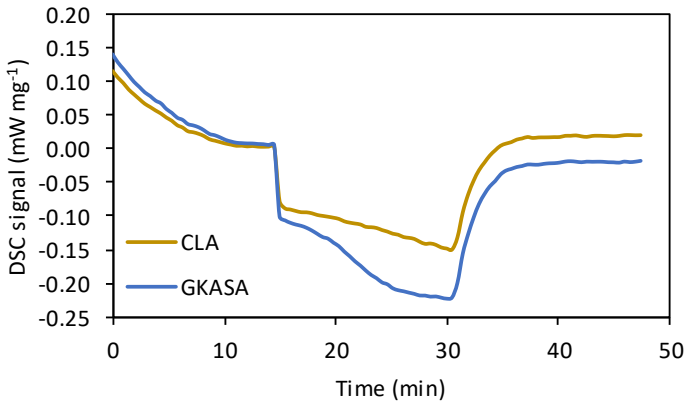

Figure 6. DSC measurements for activated carbons CLA and GKASA.

Figure 6 shows the DSC signals of the samples GKASA and CLA. A shoulder is observed in the DSC signal of GKASA (t≈ 20-30 min that corresponds to the temperature range 89-186 ˚C) that would confirm the presence of oxidation reactions on the surface of the biomass-derived carbons. This is characterised by an exothermic response upon heating. The phenolic resin derived carbon, CLA, shows the expected trend upon heating for a non-reactive process [33].

In this study the operating temperatures for the experimental *Cp* measurements have been selected so as to reproduce those that would be encountered in TSA operation for CO_2 capture. Thus, the variability observed in the performance of the evaluated carbons, i.e., phenolic resin-derived *vs*. biomass-derived, is a relevant outcome. The heat balance of the process should definitely consider the particular dependence of the heat capacity of the carbon with temperature. The synthesis protocol of the phenol-formaldehyde resin does not influence the specific heat capacity of the resultant activated carbons that exhibit similar trends; however, in the almond shells and olive stones-derived carbons the presence of biomass favours the occurrence of oxidation reactions in the presence of air and residual moisture.

3.1.2 Influence of different activating agents used in biomass-derived ACs

A commercial activated carbon, Norit C (Cabot Europe), was tested in order to evaluate the influence of different activating agents, i.e., physical activation versus chemical activation, on the specific heat capacity. This activated carbon is obtained from wood by means of chemical activation with phosphoric acid at 550 ˚C [30]. Due to its biomass origin, its thermal behaviour is compared with that of GKASA, which is also a biomass-derived AC but it has been developed by physical activation with carbon dioxide.

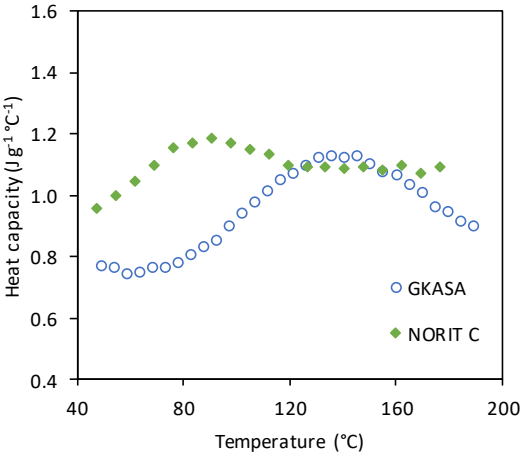

Figure 7. Specific heat capacities of biomass-based carbons prepared with different activating agents.

As can be observed in Figure 7, both samples display similar *Cp* behaviour with temperature to that previously reported in Section 3.1.1 for a biomass-derived carbon. The chemically activated carbon, Norit C, shows higher specific heat capacity up to ~100 ˚C, probably attributed to the nature of the phosphoric acid treatment that promotes an acidic character of the AC [45,46], as opposed to the basic character associated to CO_2 activation [29,47]. Uddin et al [33], reported lower specific heat capacity values for Maxsorb III than for the corresponding samples post-treated with H_2 and KOH-H_2.

It has been found that oxygen surface functionalities contribute to the overall specific heat capacity of the sample and the role of carboxylic groups seems particularly relevant to the observed increase in heat capacity [33,38]. As reported by Wang et al. [44], the decomposition of unstable oxygenated intermediates formed during oxidation reactions primarily generates CO_2. As time progresses, accumulation of stable oxygenated complexes, including hydroxyl and carboxyl groups, at the surface of activated carbon pores retards chemisorption and results in a considerable decrease in CO_2 production. With the deactivation of reaction sites for oxygen chemisorption, the thermal decomposition of stable oxygenated complexes becomes the limiting step of the chemisorption process. The vast majority of reaction sites in Norit C seem to contribute to the formation of carboxyl (COOH) groups upon oxidation that are thermally more labile. This could account for the shifting of the peak in Figure 7 to lower temperatures (80 ˚C). On the contrary, sample GKASA probably possesses a greater number of sites which lead to the formation of more stable species like carbonyl (CO) groups, thus displacing the thermal decomposition to higher temperatures (150 ˚C).

3.1.3 Influence of adsorbent surface modifications

Two different materials, a char obtained from almond shells (GKAS) and a commercial activated carbon (Norit C), and their surface-modified counterparts (GKASN, GKASA, CNO and CN) have been selected to investigate the influence of different surface modification treatments on *Cp* values.

Sample GKAS was obtained by carbonisation in nitrogen atmosphere (flow rate of 50 mL/min) up to a maximum temperature of 600 ˚C with a soaking time of 30 min [28]. Subsequently, it was

subjected to either direct amination without prior oxidation yielding GKASN sample, or to physical activation with CO_2, from which GKASA was obtained [29].

Samples CNO and CN were prepared from Norit C by ammoxidation and amination treatments, respectively, which are further explained elsewhere [31].

In order to study the influence of the treatments on the acid-base properties of the carbon surfaces, the estimation of the point of zero charge (pH_{PZC}) was accomplished by a mass titration method adapted from Noh and Schwarz [48,49].

As can be seen in Table 2, the pH values indicate that GKAS-derived carbons present a basic character. Basicity after activation with CO_2 may be due to basic oxygen functionalities incorporated to the surface of the char [50] or to Lewis type basic sites associated to the carbon structure [51]. As expected, amination produced the most basic sample with an increase of 21% in pH_{PZC} observed for GKASN [28] with regards to GKASA (pH_{PZC}=9.9).

Table 2. Point of zero charge of GKAS and Norit C derived ACs.

Sample	Precursor		Treatment		pH_{PZC}
	Origin	Type	Type	Agent	
GKASA	GKAS	--	Physical Activation	CO_2	9.9
GKASN	GKAS	--	Amination	NH_3	12.0
Norit C	Biomass	Wood	Chemical Activation	H_3PO_4	2.8
CNO	Norit C	--	Ammoxidation	NH_3 +Air	6.1
CN	Norit C	--	Amination	NH_3	8.9

Conversely, the point of zero charge of Norit C (pH_{PZC} = 2.8) evidences its acidic character. By means of ammoxidation treatment a pH_{PZC} increase of 118% is attained in CNO whereas amination changes the character of Norit C from strongly acidic to basic, resulting in an increment of 218% in pH_{PZC} of CN.

Measurement of *Cp* values for all the samples summarised in Table 2 showed the already reported shoulder (see Figure 8) that has been ascribed to oxidation reactions in the previous sections. It is worth to note that as the surface becomes more basic the specific heat capacity of the GKAS-derived carbons decreases, with the lowest values being achieved for the GKASN sample.

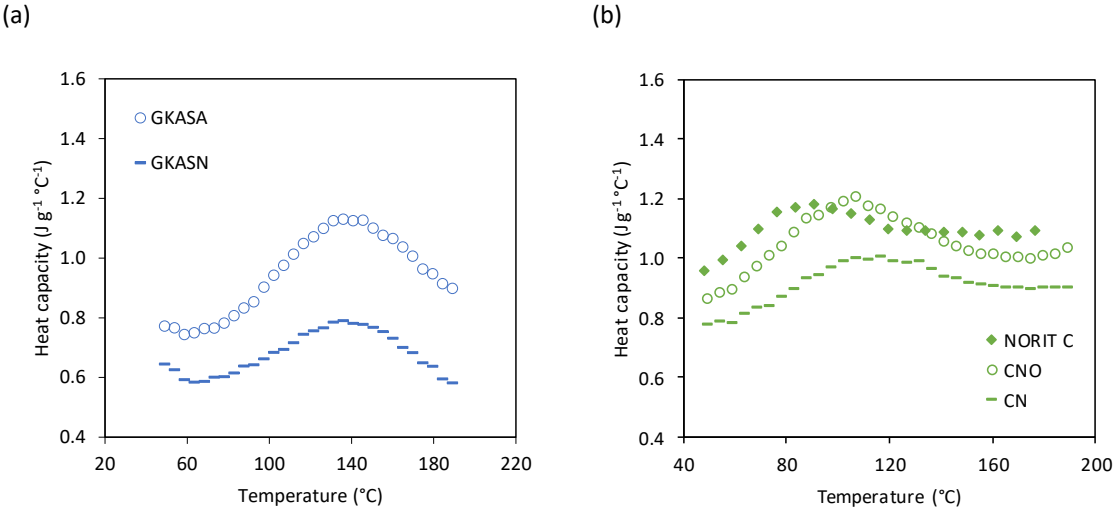

Figure 8. Specific heat capacity of samples: (a) GKASA and GKASN and (b) Norit C, CNO and CN.

For Norit C derived carbons, the parent carbon C and the ammoxidised sample CNO showed similar values of specific heat capacity over the studied temperature range, whereas the ammonia treated sample CN showed similar trend but at lower values of specific heat capacity. Contrary to the GKAS derived carbons, their specific heat capacities seem to be influenced by the pH_{PZC} values to a lesser extent.

Findings from this section suggest that adsorbent surface modification influences heat capacity and could play an important role in tailoring adsorbents with suitable specific heat capacities for TSA processes.

3.2 Implications for Thermal Swing Adsorption (TSA) processes

Post-combustion flue gas can be released, after desulphurisation, at a temperature in the range of 40 to 60 ˚C and close to atmospheric pressure, wherein CO_2 is present at a relatively low partial pressure of 0.13–0.16 bar. Thus, the capacity to adsorb CO_2 in the low-pressure region is critically important [52].

Capturing CO_2 with solid adsorbents can be often limited by heat transfer during the regeneration process rather than mass transfer during the adsorption process [53]. As explained before, the use of a low-heat capacity adsorbent would result in a lower energy penalty for the regeneration step, which would be of significant benefit for reducing the total energy cost of post-combustion CO_2 capture.

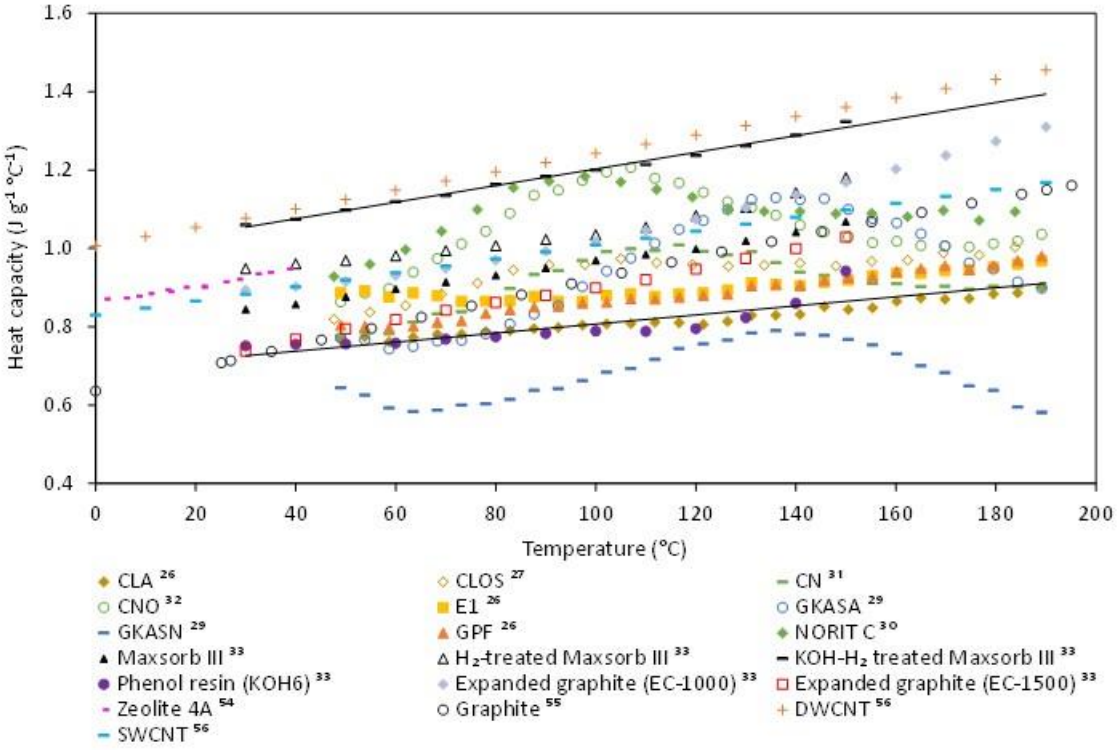

Figure 9. Comparison of the specific heat capacity of the studied activated carbon materials and other carbon-based materials previously reported in literature.

In this study, the specific heat capacities of several activated carbons, such as phenolic resin-derived carbons (CLA, CLOS, E1 and GPF) and biomass-based carbons (Norit C, CN, CNO, GKASA and GKASN) suitable for CO_2 capture by means of adsorption have been evaluated experimentally and all the data are plotted for a temperature range from 50 to 190 ˚C in Figure 9. Available data in the literature for reference materials like zeolites [54], graphite [33,55], carbon nanotubes [56], etc., are also plotted for benchmarking purposes. It is important to note that sample GKAS has not been included because it is a char, not an activated carbon.

The specific heat capacities of the evaluated adsorbents evidence significant dependency on temperature as reported in [33,38,40]. Globally, specific heat capacities increase approximately linearly with temperature, in the evaluated temperature range, except for the biomass-based carbons that show a peak at intermediate temperatures that is ascribed to oxidation during the experiment.

Defining an operation window wherein the lower and upper bounds are the specific heat capacities displayed by KOH6-PR and KOH-H_2, treated Maxsorb III studied by Uddin et al. [33], we can appreciate that the vast majority of the activated carbons experimentally evaluated in this study are within this window (1.0 to 1.3 J/(g ˚C) for the upper limit and 0.7 to 0.8 J/(g ˚C) for the lower limit) and exhibit comparable values to expanded graphite, zeolites or single-wall carbon nanotubes (SWCNT).

Most of the literature on carbon-based adsorption processes applied to CO_2 capture has usually adopted an average value of *Cp* of approximately 1.0 J/(g ˚C) [7] for the estimation of the sensible heat, taking as a reference the specific heat capacity measured for graphite (0.71 J/(g ˚C) at 22 °C [57]); this is in agreement with the results obtained in this study. In addition to the sensible heat, the energy duty for desorption during regeneration in a TSA process based on physisorbents, like the carbon-based materials studied herein, mainly depends on the heat of desorption [58,59]. Thus, developing materials with increased CO_2 loading, low specific heat capacity and lower heat of adsorption can lead to a more efficient capture technology [59]. Berlier et al. [60], reported a heat of CO_2 adsorption on an activated carbon of $\sim$ 3 kJ/mol CO_2 at 25 °C and 1 bar which indicates low energy requirement during regeneration to counteract the endothermic desorption. This value is low compared to the more recently reported for carbon-based adsorbents, 15-30 kJ/mol CO_2 [2,61,62].

The use of carbon-based adsorbents is however associated to lower CO_2 adsorption capacity which in turn means larger adsorbent inventory and, therefore, more heat for regeneration; however, since carbon-based adsorbents are expected to have longer lives and may not require additional SO_2 scrubbing, they are still appealing options, particularly if further improvements in working CO_2 capacity are achieved [6].

The desorption temperature required in the regeneration step of a TSA process depends on the specific configuration of the plant and could be as high as 200 ˚C [52]. Tlili et al. [63], using zeolite 5A as adsorbent, concluded that the CO_2 flow rate recovered depends on the regeneration temperature: it reaches a maximum value with increasing temperature up to a certain set point and then decreases slowly showing a tail. A large part of the adsorbed CO_2 (80%) could be recovered at atmospheric pressure and 210 ˚C. Furthermore, Pirngruber et al. [64], determined that the optimum regeneration

377 temperature, i.e., the temperature that minimises the overall energy consumption, for a solid adsorbent
378 with a heat of CO_2 adsorption of around 50 kJ/mol and a maximum adsorption capacity of 2.9 mol
379 CO_2/kg is around 177 ˚C.

380 It is noteworthy that sample GKASN shows the lowest specific heat capacity at 190 ˚C,
381 0.58 J/(g ˚C), amongst all studied activated carbons. As explained above in Section 3.1.3, this may be the
382 result of its stronger basic character (pH_{PZC} of 12.0). On the other hand, Norit C presents the highest Cp
383 value, 1.09 J/(g ˚C), due to its most acidic character (pH_{PZC} of 2.8). Likewise, this value remains slightly
384 lower than those attained by other carbon materials such as graphite [55] and SWCNT [56] with around
385 1.15 J/(g ˚C), and DWCNT [56] with 1.46 J/(g ˚C) at the same temperature (see Figure 9).

386 Many parameters could influence the specific heat capacity values. The experimental protocol
387 and pre-treatment conditions (i.e., drying) are crucial in the estimation. Besides, the particle size of the
388 carbon materials could also influence. In this study, all the samples evaluated were in fine powder form
389 (ground in an Agate mortar).

390 The effect of the textural characteristics of the ACs on the specific heat capacity has also been
391 investigated. For this purpose, characterisation by standard CO_2 adsorption was performed up to a
392 relative pressure $p/p^0 \sim 0.030$ at 0 °C (Micromeritics TriStar 3000). The adsorption of CO_2 at 0 °C and up
393 to atmospheric pressure assesses microporosity narrower than 1 nm. The analysis of the CO_2 adsorption
394 data by means of the linearised Dubinin-Astakhov (DA) equation [65] leads to the corresponding volume of
395 micropores (W_0) and characteristic energy (E_0) (Table 3).

396 **Table 3.** Textural properties of the activated carbons (CO_2, 0 °C) and *Cp* values at 190 °C.

Adsorbent	W_0	E_0	L_0	*Cp*
CLA	0.28	26.17	0.73	0.90
CLOS	0.25	28.68	0.62	1.00
E1	0.30	26.77	0.70	0.97
GPF	0.26	26.81	0.70	0.98
GKASA	0.32	27.65	0.66	0.90
GKASN	0.19	33.10	0.50	0.58
Norit C	0.33	22.50	0.97	1.09
CN	0.37	23.69	0.88	0.90
CNO	0.15	28.97	0.61	1.04

397 W_0 [=] cm^3/g; E_0 [=] kJ/mol; L_0 [=] nm; *Cp* [=] J/(g ˚C)

398 The CO_2 capture capacity is directly linked to these parameters [66] and the average width of the
399 corresponding micropores is related to the characteristic energy by means of the Stoeckli-Ballerini
400 relation, L_0=10.8/(E_0-11.4). The specific heat capacity values of the samples at the maximum
401 temperature of 190 ˚C evaluated in this study *versus* W_0 and L_0 are presented in Figure 10.

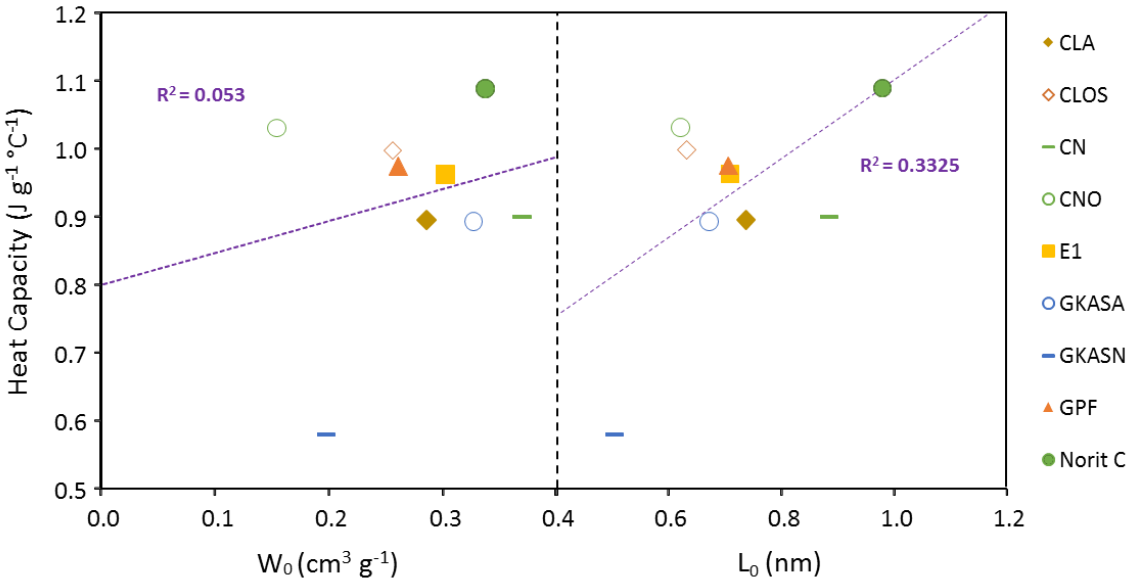

Figure 10. Specific heat capacity *vs* CO_2 textural parameters (W_0 and L_0) of the activated carbons studied.

It becomes apparent that there is not a specific correlation between the narrow micropore volume (W_0) and width (L_0) and the specific heat capacity. Besides, the influence of the textural parameters in the specific heat capacity of carbons has not been reported in the literature.

On the other hand, the role of surface functionalities and, particularly, the acid and basic character of the carbon surface has been identified as key parameter. Thus, the specific heat capacity values of the samples, at the maximum temperature of 190 ˚C evaluated in this study, *versus* the point of zero charge are presented in Figure 11. It can be observed that the majority of the carbon samples evaluated in this study have basic character.

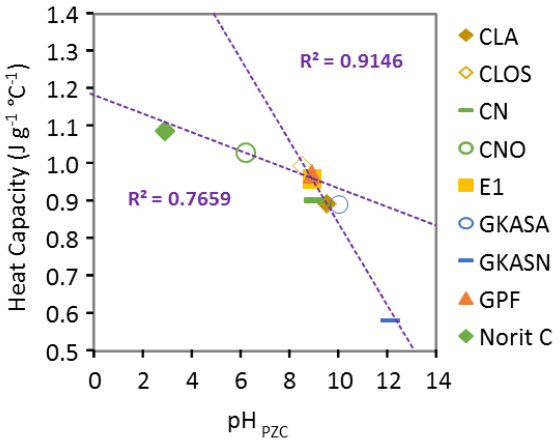

Figure 11. Specific heat capacity *vs* point of zero charge of the activated carbons studied.

Globally, the increase in specific heat capacity with the acidity of the samples, represented by low pH_{PZC} values, would suggest a specific contribution of acidic surface oxygen functional groups (Figure 11); however, no clear proportionality is observed. The best correlation is found for pH_{PZC} values smaller than 8.9 but data scattering is still remarkable. For a sample's basicity between 8.9 and 9.9 and,

independently of the precursor of the carbon sample, the specific heat capacity at 190 ˚C remains approximately constant at a value of 0.90 J/(g ˚C).

As can be seen in Figure 11, activated carbons with pH_{PZC} values higher than 9 are low-heat capacity adsorbents (< 1 J/(g ˚C)), very appealing for effective regeneration in TSA processes, whilst AC adsorbents with an acidic character may be undesirable owing to their higher specific heat capacities. Nevertheless, it is important to note that there exists a trade-off between the easiness of the regeneration and the CO_2 adsorption capacity of the adsorbents.

4 Conclusions

The specific heat capacities of several carbon-based adsorbents suitable for post-combustion CO_2 capture have been evaluated experimentally over a wide temperature range, 50 to 190 ˚C, which is the practical operation window for thermal swing adsorption in post-combustion CO_2 capture processes.

The selected solid adsorbents include examples of ACs prepared from different precursor materials, synthesis conditions, activating agents and surface modifications, so the study covers a wide range of preparation conditions.

The specific heat capacities of the evaluated adsorbents evidence significant dependency on temperature. Phenolic resin-derived carbons followed the expected trend characterised by a slight increase of the heat capacity with temperature in the 50 to 190 ˚C range. No particular influence of the synthesis protocol was observed. However, when the carbon precursor contained biomass the pattern changed and a peak in the heat capacity *vs*. temperature plot was observed. It was ascribed to oxidation reactions occurring during the experiment.

An important finding from this study was that adsorbent surface modification plays a key role in the specific heat capacity of resultant carbons as chemically-activated ACs, i.e., most acidic ones, showed the highest specific heat capacity values. Activated carbons with pH_{PZC} values higher than 9 showed low-heat capacity (< 1 J/(g ˚C)) very suitable for effective regeneration in TSA processes.

Specific correlations between the textural characteristics of the carbons and the estimated heat capacity values have not been found but the acid and basic character of the carbon surface has been identified as key parameter. This is an important finding to tailor materials with the desired properties for a more energy-efficient regeneration process.

Acknowledgements

N.Q. acknowledges a fellowship from the Gobierno del Principado de Asturias (Programa Severo Ochoa).

References

1 J. Wilcox, *Carbon capture*, Springer New York, New York, NY, 2012.

2 A. Samanta, A. Zhao, G. K. H. Shimizu, P. Sarkar and R. Gupta, *Industrial and Engineering Chemistry Research*, 2012, **51**, 1438–1463.

3 Q. Wang, J. Luo, Z. Zhong and A. Borgna, *Energy Environ. Sci.*, 2011, **4**, 42–55.

4 D. M. D'Alessandro, B. Smit and J. R. Long, *Angewandte Chemie International Edition*, 2010, **49**, 6058–6082.

5 H. W. Pennline, D. R. Luebke, K. L. Jones, C. R. Myers, B. I. Morsi, Y. J. Heintz and J. B. Ilconich, *Fuel Processing Technology*, 2008, **89**, 897–907.

6 S. Sjostrom and H. Krutka, *Fuel*, 2010, **89**, 1298–1306.

7 M. Radosz, X. Hu, K. Krutkramelis and Y. Shen, *Industrial and Engineering Chemistry Research*, 2008, **47**, 3783–3794.

8 C. M. Quintella, S. A. Hatimondi, A. P. S. Musse, S. F. Miyazaki, G. S. Cerqueira and A. De Araujo Moreira, *Energy Procedia*, 2011, **4**, 2050–2057.

9 E. Blomen, C. Hendriks and F. Neele, *Energy Procedia*, 2009, **1**, 1505–1512.

10 B. Li, Y. Duan, D. Luebke and B. Morreale, *Applied Energy*, 2013, **102**, 1439–1447.

11 L. Espinal, D. L. Poster, W. Wong-Ng, A. J. Allen and M. L. Green, *Environmental Science and Technology*, 2013, **47**, 11960–11975.

12 B. Sreenivasulu, D. V. Gayatri, I. Sreedhar and K. V. Raghavan, *Renewable and Sustainable Energy Reviews*, 2015, **41**, 1324–1350.

13 A. Sayari, Y. Belmabkhout and R. Serna-Guerrero, *Chemical Engineering Journal*, 2011, **171**, 760–774.

14 S. Y. Lee and S. J. Park, *Journal of Industrial and Engineering Chemistry*, 2015, **23**, 1–11.

15 A. E. Creamer and B. Gao, *Environmental Science & Technology*, 2016, **50**, 7276–7289.

16 A. A. Olajire, *Energy*, 2010, **35**, 2610–2628.

17 R. Ben-Mansour, M. A. Habib, O. E. Bamidele, M. Basha, N. A. A. Qasem, A. Peedikakkal, T. Laoui and M. Ali, *Applied Energy*, 2016, **161**, 225–255.

18 M. Songolzadeh, M. Soleimani, M. Takht Ravanchi and R. Songolzadeh, *The Scientific World Journal*, 2014, **2014**, 828131.

19 D. Cebrucean, V. Cebrucean and I. Ionel, *Energy Procedia*, 2014, **63**, 18–26.

20 B. P. Spigarelli and S. K. Kawatra, *Journal of CO_2 Utilization*, 2013, **1**, 69–87.

21 M. Bui, C. S. Adjiman, A. Bardow, E. J. Anthony, A. Boston, S. Brown, P. S. Fennell, S. Fuss, A. Galindo, L. A. Hackett, J. P. Hallett, H. J. Herzog, G. Jackson, J. Kemper, S. Krevor, G. C. Maitland, M. Matuszewski, I. S. Metcalfe, C. Petit, G. Puxty, J. Reimer, D. M. Reiner, E. S. Rubin, S. A. Scott, N. Shah, B. Smit, J. P. M. Trusler, P. Webley, J. Wilcox and N. Mac Dowell, *Energy & Environmental Science*, 2018, **11**, 1062–1176.

22 N. Sundaram and R. T. Yang, *Journal of Colloid and Interface Science*, 1998, **198**, 378–388.

23 B. Smit, J. A. Reimer, C. M. Oldenburg and I. C. Bourg, *Introduction to Carbon Capture and Sequestration*, IMPERIAL COLLEGE PRESS, 2014, vol. 1.

24 S. Choi, J. H. Drese and C. W. Jones, *ChemSusChem*, 2009, **2**, 796–854.

25 C. H. Yu, C. H. Huang and C. S. Tan, *Aerosol and Air Quality Research*, 2012, **12**, 745–769.

26 C. F. Martín, M. G. Plaza, S. García, J. J. Pis, F. Rubiera and C. Pevida, *Fuel*, 2011, **90**, 2064–2072.

27 N. Álvarez-Gutiérrez, M. Gil, M. Martínez, F. Rubiera and C. Pevida, *Energies*, 2016, **9**, 189.

28 M. G. Plaza, C. Pevida, B. Arias, J. Fermoso, F. Rubiera and J. J. Pis, *Energy Procedia*, 2009, **1**, 1107–1113.
29 M. G. Plaza, C. Pevida, C. F. Martín, J. Fermoso, J. J. Pis and F. Rubiera, *Separation and Purification Technology*, 2010, **71**, 102–106.
30 Powdered Activated Carbon | Cabot Corporation, http://www.cabotcorp.com/solutions/products-plus/activated-carbon/powdered, (accessed 26 October 2017).
31 C. Pevida, M. G. Plaza, B. Arias, J. Fermoso, F. Rubiera and J. J. Pis, *Applied Surface Science*, 2008, **254**, 7165–7172.
32 M. G. Plaza, F. Rubiera, J. J. Pis and C. Pevida, *Applied Surface Science*, 2010, **256**, 6843–6849.
33 K. Uddin, M. Amirul Islam, S. Mitra, J. boong Lee, K. Thu, B. B. Saha and S. Koyama, *Applied Thermal Engineering*, 2018, **129**, 117–126.
34 K. L. Ramakumar, M. K. Saxena and S. B. Deb, *Journal of Thermal Analysis and Calorimetry*, 2001, **66**, 387–397.
35 D. A. Ditmars, S. Ishihara, S. S. Chang, G. Bernstein and E. D. West, *Journal of Research of the National Bureau of Standards*, 1982, **87**, 159.
36 M. J. Richardson, *Thermochimica Acta*, 1997, **300**, 15–28.
37 T. A. Tip, *Interpreting DSC curves Part 1: Dynamic measurements Information for users of METTLER TOLEDO thermal analysis systems*, 2000.
38 B. Mu and K. S. Walton, *Journal of Physical Chemistry C*, 2011, **115**, 22748–22754.
39 S. Rudtsch, *Thermochimica Acta*, 2002, **382**, 17–25.
40 M. Kano, M. Momota, T. Okabe and K. Saito, *Elsevier Thermochimica Acta*, 1997, **292**, 175–177.
41 H. Wang, B. Z. Dlugogorski and E. M. Kennedy, *Progress in Energy and Combustion Science*, 2003, **29**, 487–513.
42 S. Loganathan, R. B. Valapa, R. K. Mishra, G. Pugazhenthi and S. Thomas, in *Thermal and Rheological Measurement Techniques for Nanomaterials Characterization*, Elsevier, 2017, pp. 67–108.
43 S. Lagorsse, M. C. Campo, F. D. Magalhães and A. Mendes, *Carbon*, 2005, **43**, 2769–2779.
44 H. Wang, B. Z. Dlugogorski and E. M. Kennedy, *Energy and Fuels*, 2003, **17**, 150–158.
45 S. Yorgun and D. Yildiz, *Journal of the Taiwan Institute of Chemical Engineers*, 2015, **53**, 122–131.
46 J. Kazmierczak-Razna, P. Nowicki, M. Wiśniewska, A. Nosal-Wiercińska and R. Pietrzak, *Journal of the Taiwan Institute of Chemical Engineers*, 2017, **80**, 1006–1013.
47 M. G. Plaza, A. S. González, C. Pevida, J. J. Pis and F. Rubiera, *Applied Energy*, 2012, **99**, 272–279.
48 J. P. Reymond and F. Kolenda, *Powder Technology*, 1999, **103**, 30–36.
49 J. S. Noh and J. A. Schwarz, *Journal of Colloid and Interface Science*, 1989, **130**, 157–164.
50 E. Papirer, S. Li and J. B. Donnet, *Carbon*, 1987, **25**, 243–247.
51 C. A. Leon y Leon, J. M. Solar, V. Calemma and L. R. Radovic, *Carbon*, 1992, **30**, 797–811.
52 J. A. Mason, K. Sumida, Z. R. Herm, R. Krishna and J. R. Long, *Energy & Environmental Science*,

2011, **4**, 3030.

53 J. S. Bae and S. Su, *International Journal of Greenhouse Gas Control*, 2013, **19**, 174–182.

54 L. Qiu, V. Murashov and M. A. White, *Solid State Sciences*, 2000, **2**, 841–846.

55 A. T. D. Butland and R. J. Maddison, *Journal of Nuclear Materials*, 1973, **49**, 45–56.

56 G. G. Silva, A. W. Musumeci, A. P. Gomes, J. W. Liu, E. R. Waclawik, G. a George, R. L. Frost and M. A. Pimenta, *Journal of Materials Science*, 2009, **44**, 3498–3503.

57 S. Picard, D. T. Burns and P. Roger, *Rapport BIPM-2006/01: Measurement of the specific heat capacity of graphite*, 2006.

58 C. Goel, H. Bhunia and P. K. Bajpai, *RSC Advances*, 2015, **5**, 93563–93578.

59 M. Clausse, J. Merel and F. Meunier, *International Journal of Greenhouse Gas Control*, 2011, **5**, 1206–1213.

60 K. Berlier and M. Frère, *Journal of Chemical & Engineering Data*, 2002, **41**, 1144–1148.

61 B. Guo, L. Chang and K. Xie, *Journal of Natural Gas Chemistry*, 2006, **15**, 223–229.

62 Q. Cen, M. Fang, T. Wang, I. Majchrzak-Kucęba, D. Wawrzyńczak and Z. Luo, *Greenhouse Gases: Science and Technology*, 2016, **6**, 787–796.

63 N. Tlili, G. Grévillot and C. Vallières, *International Journal of Greenhouse Gas Control*, 2009, **3**, 519–527.

64 G. D. Pirngruber, F. Guillou, A. Gomez and M. Clausse, *International Journal of Greenhouse Gas Control*, 2013, **14**, 74–83.

65 H. F. Stoeckli, *Carbon*, 1981, **19**, 325–326.

66 N. Querejeta, M. V. Gil, C. Pevida and T. A. Centeno, *Journal of CO_2 Utilization*, 2018, **26**, 1–7.